



# Drop-Weight Impact Behavior of Three-Dimensional Printed Polymer Lattice Structures with Spatially Distributed Vertical Struts

M. Al Rifaie<sup>1</sup> · A. Mian<sup>1</sup> · P. Katiyar<sup>2</sup> · P. Majumdar<sup>2</sup> · R. Srinivasan<sup>1</sup>

Received: 14 November 2018 / Accepted: 30 May 2019 / Published online: 4 June 2019  
© Society for Experimental Mechanics, Inc 2019

## Abstract

Three-dimensional (3D) printed polymer lattice structures of different configurations are investigated in this research to study their behavior under low-velocity impact load. The Body Centered Cubic (BCC) is modified and redesigned to generate three additional sets of the lattice structures to compare their impact energy absorption capability. The modified designs are (a) BCC with vertical struts connecting all nodes (BCCV) (b) BCC with vertical bars connecting alternate nodes (BCCA), and (c) BCC with gradient distribution of struts (BCCG). All the four sets are created using Acrylonitrile Butadiene Styrene (ABS) polymer material on a Stratasys uPrint 3D printer. An in-house built ASTM Standard D7136 drop tester was used to capture the impact response. Data obtained from the attached accelerometer is post processed to find velocity, displacement, transferred energy, and force histories. The absorbed energy is found from the change in kinetic energy of the impactor before and after impact. It is observed that the selective placement of vertical support struts in the thickness direction influences the impact response of lattice structures.

**Keywords** Additive manufacturing · 3D printing · Energy absorption · Lattice structures · Low velocity impact

## Introduction

Cellular structures are a combination of solid material and air. These structures are available in nature like cork and are made by conventional methods like honeycomb. In addition, lattice structures are another type of cellular structure that can be either 3D printed or made. Lattice structures (LS) are a group of small unit cell structures arranged next to each other over a space. They have great mechanical properties, such as being lightweight, having high strength-to-weight ratio, and having good energy absorption capability [1–6]. Owing to the recent advent of the three-dimensional printing (3DP) processes, several studies of metallic LS under impact loading have concluded that lattice core structures have impact performance comparable to honeycomb structures, and that improvements to the performance can be achieved through improved material and architectural

combinations of the lattice core [2–6]. Cellular structures including ordered and stochastic cellular structures can be created by using conventional methods. For example, a man-made honeycomb is an ordered cellular structure that can be manufactured by joining the corrugated sheet and arranging them to build up the hexagonal shapes [7]. Stochastic cellular structures can be made more easily than ordered cellular structures. There are several examples including metal sponges, metal foams and hollow sphere foams that are produced by distributing the voids stochastically [8] during manufacturing.

Over last several years, researchers have used several methods such as photopolymerization using collimated UV light and mask with apertures to create lattice structures [4]; however, the 3DP method is currently being explored because of its flexible nature of fabrication [5, 6, 9]. Three-dimensional printing (3DP), an Additive Manufacturing (AM) process, has rapidly grown in recent years and has been widely used in many applications. The 3DP manufacturing process requires an input file usually in STereoLithography (STL) format generated by a CAD software to build complex models. From the STL file, the printer software creates toolpath, and prints the model layer by layer. There are several AM technologies, however extrusion-based process

✉ A. Mian  
ahsan.mian@wright.edu

<sup>1</sup> Department of Mechanical and Materials Engineering,  
Wright State University, Dayton, OH, USA

<sup>2</sup> Department of Mechanical Engineering, University of South  
Carolina, Columbia, SC, USA

widely known as Fused Deposition Modeling (FDM) is the most used one for plastics due to its low-cost. The print head extrudes the filament through the heated nozzle that solidifies when it reaches build platform [10–15]. Due to the flexible layering nature of manufacturing, the 3DP process can be used to fabricate intricate parts with internal features of great complexity. For example, the basic BCC lattice can be redesigned by adding spatially distributed vertical and horizontal struts to control its behavior and capability of strain energy absorption for any specific application.

The total absorbed energy by a structure is typically evaluated by taking the difference between the incident kinetic energy and residual kinetic energy of the impactor tip when impact test is used [16]. However, the nature of absorbed energy variation during the loading event, which is also important for some applications, cannot be obtained from the incident and residual kinetic energies. Energy absorption capability of cellular structures under low-velocity impact tests has been investigated by many researchers [2, 9, 17–19]. St-Pierre et al. [17] performed a low-speed impact test on Y-frame and corrugated sandwich beams. The drop-weight responses were comparable to the ones measured quasi-statically. Vesjenjak, et al. [18] performed experimental and computational investigation of regular open-cell cellular structures under impact loading. Open-cell cellular specimens made of aluminum alloy and polymer were experimentally tested under quasi-static and dynamic compressive loading in order to evaluate the failure conditions and the strain rate sensitivity. Very limited work is done on the low-velocity impact behavior of 3D printed metallic [5, 6] and polymeric [9] lattice structures. Mines, et al. [5] and Shen, et al. [6] investigated the effect of selective laser melting (SLM) process parameters on the impact response of stainless steel and titanium lattice structures. Their focus was BCC and BCCZ (BCC with struts added in the thickness direction) lattice structures. Turner, et al. [9] studied a modified BCC structure with vertical struts added in the thickness direction alternate nodes. The structures were created using Acrylonitrile Butadiene Styrene (ABS) polymer material on a fused deposition modeling (FDM) 3D printer.

Due to the flexible nature of fabrication, the 3DP methods can be used to design lattice structures with abundant design variability. There has been some effort in creating 3D printed lattice structures [5, 6, 9]; however, it requires more research with different design possibilities of LS to utilize the full capability of 3DP. In this study, polymer lattice structures of Body Centered Cubic unit cell (BCC) and its three different variations are used to understand their behavior under a low-velocity impact load. The Body Centered Cubic (BCC) is modified and redesigned to generate three additional sets of the lattice structures to compare their impact energy absorption capability. The modified designs are (a) BCC with vertical struts connecting all nodes (BCCV) (b) BCC

with vertical bars connecting alternate nodes (BCCA), and (c) BCC with gradient distribution of struts (BCCG).

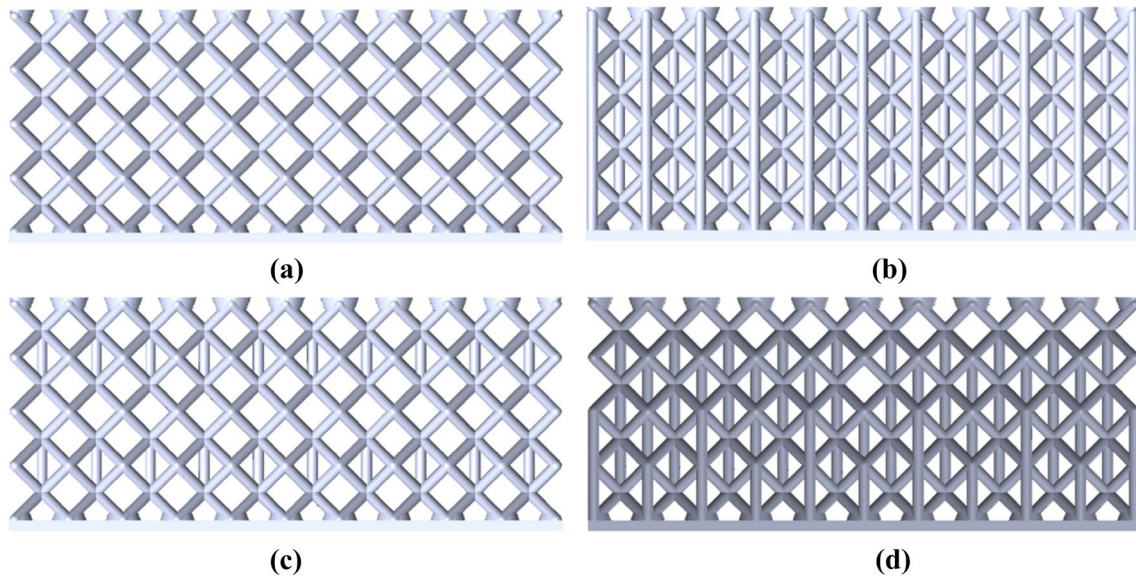
## Experimental Procedures

### Design and Fabrication of Lattice Core Structures

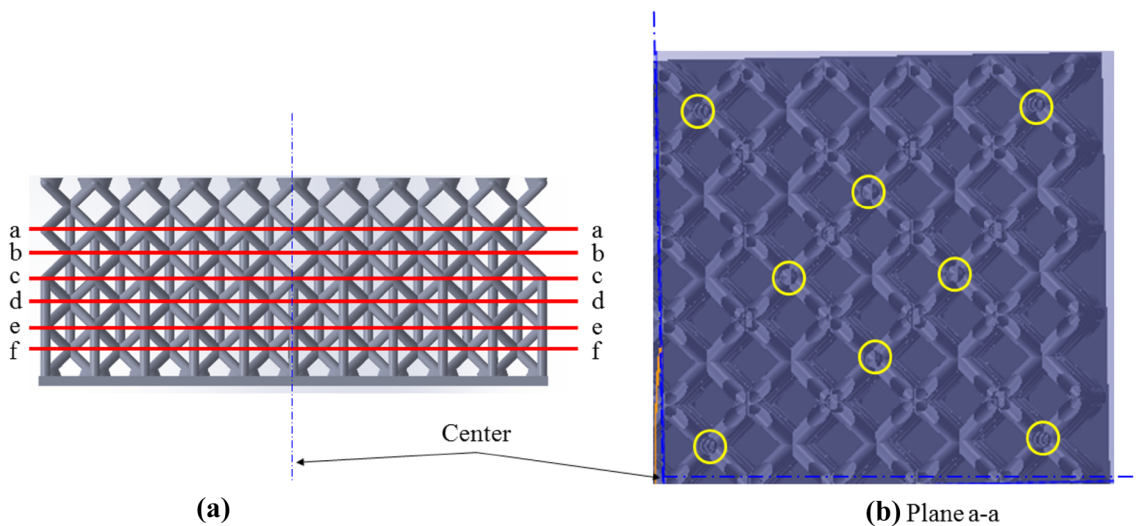
The four configurations of lattice core structures BCC, BCCV, BCCA, and BCCG were designed using a CAD software. The BCC unit cell was considered as a reference to compare with the other three configurations. The overall dimensions of the structure were 50 mm × 50 mm × 20 mm in thick, and a single unit cell had dimensions of 5 mm × 5 mm × 5 mm. The unit cells were patterned in 3D coordinate system with 10 cells in x and y-directions and 4 cells in z-direction. The total number of the unit cells for each configuration is 400 cells. The truss elements of the unit cell had a diameter of 1 mm.

Figure 1 shows the side views of the BCC, BCCV, BCCA and BCCG samples, respectively. Figure 1a shows the front view of a BCC lattice sample. Adding vertical struts to the BCC lattice structure is expected to increase the strength of the structure. One such design variation is called BCCV that is shown in Fig. 1b where the BCC structure is modified by adding vertical struts of diameter 1 mm in all nodes. Another variation of the design was to add alternative vertical struts to BCC to increase strength as well as flexibility. This configuration is termed as BCCA and is shown in Fig. 1c. It has alternating vertical struts located in between the first and second stages of the unit cells. Those struts are patterned in the xy-plane and then mirrored over the top plane. Finally, inclusion of gradient vertical struts (BCCG) introduces a new type of BCC. Figure 1d shows the side view of a BCCG lattice structure. In this case, the vertical struts are distributed linearly in the thickness direction. This design is intended to have controlled progressive failure from the weakest layer (the least number of vertical struts) to the strongest layer (the most number of vertical struts). The gradient distribution number of vertical struts in the thickness direction are shown by different planes in Fig. 2. Six different planes indicated by a–a, b–b, c–c, d–d, e–e, and f–f are shown in Fig. 2a. The total numbers of vertical struts at those planes a–a through e–e were 32, 32, 52, 59, 100, and 111, respectively. Figure 2b shows the quarter section view at Plane a–a showing the location of vertical struts indicated by yellow circles.

A fused deposition modeling (FDM) based 3D printer Stratasys uPrint SE plus [20] having a nozzle diameter of 254 μm was used to make all four designs of lattice structures. Three samples from each design totaling twelve samples were printed. An ivory-colored production-grade thermoplastic (ABSplus-P430) was used to create the samples.



**Fig. 1** Side view of four different lattice configurations: **a** BCC, **b** BCCV, **c** BCCA, and **d** BCCG



**Fig. 2** Gradient distribution of vertical struts, **a** six different planes indicated by a-a through f-f having different arrangement of vertical struts, **b** a quarter view of plane a-a showing eight vertical struts indicated by circles

The material exhibits elastic–plastic behavior both under tension and compression at room temperature [21, 22]. Mechanical properties of the material obtained under those room temperature tests performed are shown in Table 1. The material also exhibits the following thermal properties: heat deflection at 66 psi of 96 °C, glass transition temperature of 108 °C, and coefficient of thermal expansion (CTE) of  $8.82 \times 10^{-6}/^{\circ}\text{C}$  [21].

The CAD software generated STL files were processed with CatalystEX software provided by Stratasys. Three samples were printed for each design using the following printer parameters. The printer head temperature of 300 °C, and

**Table 1** Mechanical properties of ABSplus polymer

Mechanical properties	Tensile (ASTM D638) [21]	Compressive [22]
Yield strength (MPa)	31	37
Ultimate strength (MPa)	33	42
Elongation at yield (%)	2	–
Elongation at break (%)	6	21
Modulus (GPa)	2.2	1.83

the chamber temperature of 77 °C was maintained. Layer thickness was set to 0.254 mm. The models were printed using the Stratasys standard sparse high-density fill patterns where the linear scan pattern is used to create fully dense solid structure. Some samples required support materials and the amount of support material depends on the geometric complexity. The support material used in this case is a Stratasys proprietary polymeric material that is different from ABS model material. To remove the support material, a cleaning apparatus by Stratasys was used where the samples were soaked in the heated chemical bath for approximately 4 h. After removing the material, the specimens were washed by water at room temperature and were dried. The average diameter of the struts was measured to be 1.1 mm after printing.

### Kevlar Face Sheet Fabrication

The face sheets consisted of 4 layers of Hexcel Composites' K285-38"-F161 Kevlar fabric were fabricated and attached to the lattice structures. The type of Kevlar was Kev. 49 1140 fiber with a crowfoot weave. It was pre-impregnated, pre-preg, with laminate-grade epoxy resin. The cure cycle of the Kevlar consists of three stages which are heat-up, hold and cool down. A Carver hot press was used to create the four-layer face sheet. First, four ply Kevlar was lubricated with silicone oil and covered with aluminum foil. It was then held under pressure of 3 metric tons for 3 h at 220 °C. After 3 h at 220 °C, the Kevlar was kept in the hot press under pressure until it reached room temperature. Finally, the face sheet had dimensions of 105 mm × 105 mm × 0.86 mm that was equally cut into four pieces. A microscopic side view picture of a 4 ply Kevlar face sheet is shown in Fig. 3. It is clear from the image that the four layers of Kevlar were bonded and cured very well.

### Preparation of Sandwich Structures

The composite sandwich structure consists of the lattice core structure and the Kevlar face sheet. To adhere the face sheet to the core, Loctite® Epoxy Heavy Duty adhesive was used.

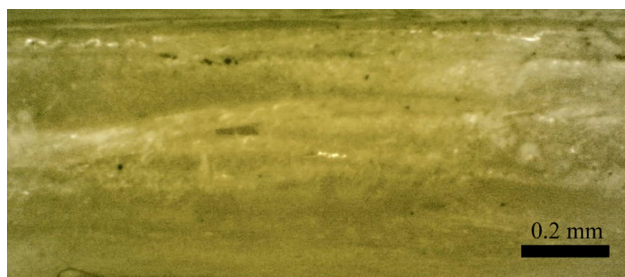


**Fig. 3** Microscopic picture of four ply Kevlar face sheet from edge

It is a two-part material that are an epoxy resin and a hardener that should be mixed in an equal amount. After mixing them, the adhesive was uniformly spread over the Kevlar face sheet and the lattice structure was placed carefully on it. The assembled composite structure was kept Kevlar face sheet down under a load of approximately 4 kg for 24 h to ensure that the adhesive is fully cured and that the face sheet is completely adhered to the core. Figure 4 shows the completed sandwich structure with BCCV lattice core. Table 2 shows the composite mass of all four configurations including the masses of Kevlar face sheets and epoxy resin. The approximated amount of the epoxy resin was 2.1 g and the Kevlar face sheets had a mass of 2.5 g.

### Low-Velocity Impact Testing

An in-house built ASTM Standard D7136/D7136M-15, low-velocity impact testing machine was used in this study [23]. It has two guide bars to make sure that the impactor hits the specimen at the center. An impactor assembly consists of proof mass and an impactor with hemispherical tip of diameter 9.5 mm (Fig. 5a). The drop height,  $h$  and proof mass,  $m$  can be adjusted to control the impact velocity and energy. In this study, the impactor assembly was dropped from a height of 0.6215 m so that the impactor reached the specimen with an incident velocity of 3.492 m/s (using  $v = \sqrt{2gh}$ ). Here, the friction due to the guide bars was considered negligible. The impactor assembly had a mass of 2.436 kg, thus the total impact energy available is the kinetic energy of the impactor assembly at the start of the impact and was calculated to be 14.85 J using Eq. (1).

$$\text{Impact energy: } KE_0 = \frac{1}{2}mv_0^2 \quad (1)$$

where  $m$  is the mass of the impactor assembly and  $v_0$  is the impactor velocity at first contact. To evaluate the absorbed

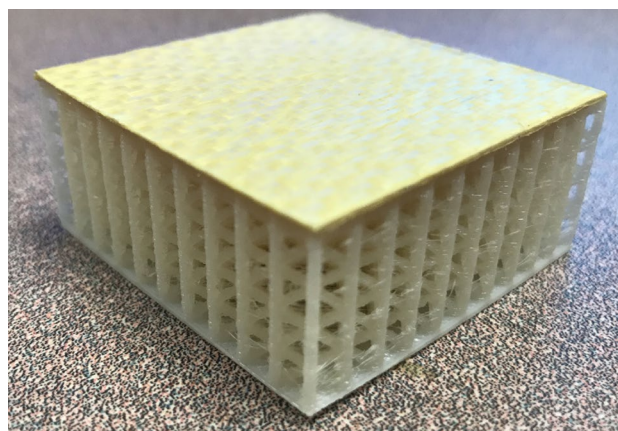


**Fig. 4** A BCCV composite sandwich structure after assembly

**Table 2** Sample characteristics for all four configurations

Configuration	BCC			BCCV			BCCA			BCCG		
Sample#	1	2	3	4	5	6	7	8	9	10	11	12
Avg. total mass (g)	18.4						19.4			19.6		

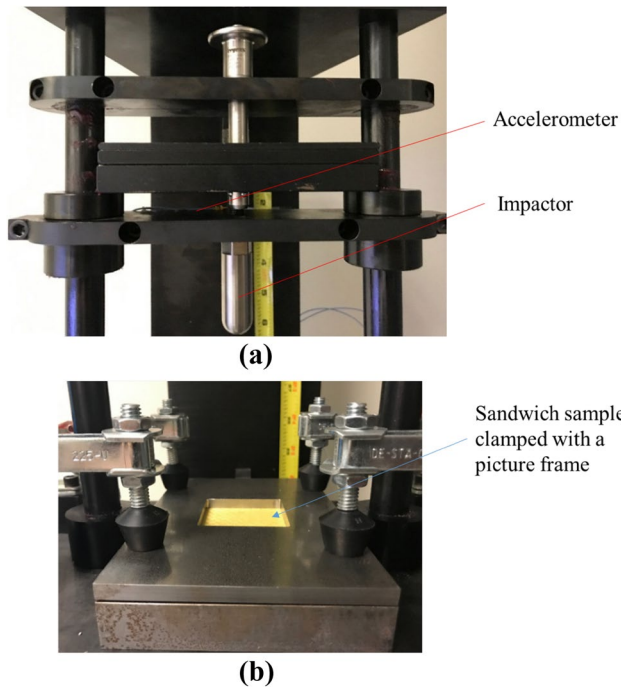


**Fig. 5** a Impactor assembly; b a sample to be impacted clamped in a fixture

energy, velocity of the impactor during impact event is needed and can be calculated by integrating the measured acceleration of the impactor over time. A piezoelectric accelerometer attached to the impactor assembly measured the acceleration history.

A fixture was designed to support the 50 mm × 50 mm specimens (Fig. 5b). The fixture uses a cutout on the test

plate to locate the specimen at the center of the impactor. The specimen sits in a 57.2 mm × 57.2 mm recess in the fixture. The entire bottom surface of the specimen was bounded from the fixture. A top plate is used to apply a downward pressure around the perimeter of the specimen using four toggle clamps.

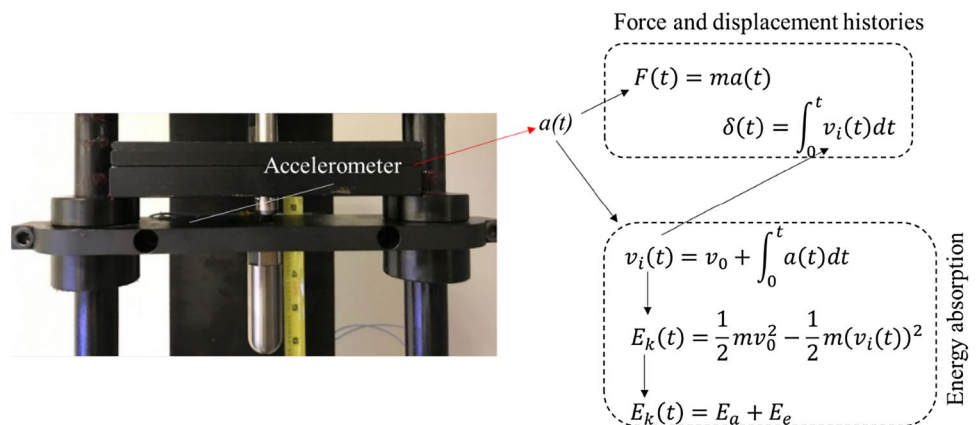
### 3D X-ray Microscopy

The 3D printed sandwich structure has a very intricate core geometry which plays a significant role in energy absorption during low velocity impact. The objective of this section is to understand the extent and mode of damage in the sandwich structure through nondestructive visualization. A 3D X-ray Computed Tomography Microscope (3D XCT microscope by Zeiss) was used which allows high resolution (0.7 μ pixel size) 3D imaging of materials. However, for this analysis, a low-resolution setup (33–38 μ pixel size) was used to capture the entire damaged volume. 3D X-ray images were taken for a representative set of specimens which provide a lucid description of the internal features of the printed substrates.

### Results and Discussion

Once the experiments of all twelve samples were complete, the acceleration data were post-processed in Matlab to determine the velocity, displacement and force histories [23] according to the calculation scheme shown in Fig. 6. The data was captured during the entire impact event or from the point of first contact ( $a = -g$ ) till the point where the

**Fig. 6** Velocity ( $v_i(t)$ ), displacement ( $\delta(t)$ ), and force histories ( $F(t)$ ), absorbed energy ( $E_a$ ), and elastic energy ( $E_e$ )



impactor just loses contact ( $a = -g$ ) with the sample. Usually, the entire test duration was 5–9 s and the impact period was about 5–7 ms. The total number of the data were about 250–350 readings. Firstly, the acceleration data obtained from the accelerometer is integrated to find impactor velocity  $v_i(t)$  at time  $t$  using Eq. (2).

$$v_i(t) = v_0 + \int_0^t a(t)dt \quad (2)$$

Here  $v_0$  is the initial impactor velocity at first contact, which was 3.492 m/s and  $a(t)$  is the measured acceleration history. Further integration of Eq. (2) gives displacement history  $\delta(t)$ . The integration starts at the first excitation point on the acceleration curve and end at the point at which the accelerometer reading is  $g$ . Integration was performed using cumulative-trapezoidal-integration algorithm. The cumulative trapezoidal (cumtrapz) method automatically smooths the data by breaking the area under the curve into infinitesimally small trapezoids. This method eliminates the need for a filter on the velocity and displacement data. Force history  $F(t)$  can be obtained by multiplying the mass of the impactor assembly  $m$  and acceleration  $a(t)$ . Energy transferred to the sample should be the same as the difference in impactor kinetic energy that was calculated in Excel using Eq. (3) as follows

$$E_k(t) = \frac{1}{2}mv_0^2 - \frac{1}{2}m(v_i(t))^2 \quad (3)$$

Thus, the energy transferred to the sample through impact is the summation of elastic energy ( $E_e$ ) and absorbed energy ( $E_a$ ) values. The elastic energy region represents the amount of the rebound energy from the specimen.

Figure 7 shows the comparison of typical velocity histories for all four configurations. There are three distinct stages in the plot, negative velocity during which the impactor moves in the downward direction after first contact up to the maximum displacement. This stage is termed as *Stage I* during which period the velocity changes from the downward velocity of 3.49 m/s to zero. *Stage II* is when the impactor changes its direction and starts moving in the upward direction due to elastic recovery of the samples. At *Stage II*, the impactor velocity is zero; however, its acceleration and displacement are maximum. The elastic recovery period of the sample is called *Stage III* during which the impactor starts moving in the upward direction (i.e. positive velocity) while being in contact with the sample. At the end of *Stage III*, the impactor separates from the sample and its acceleration becomes  $g$ .

It is clear from the figure that all configurations follow the same trend for the first millisecond of impact. This can be the response of the Kevlar face sheet in combination with the elastic deformation of the first layer of lattice. The duration of *Stage I* for BCCV and BCC samples are approximately

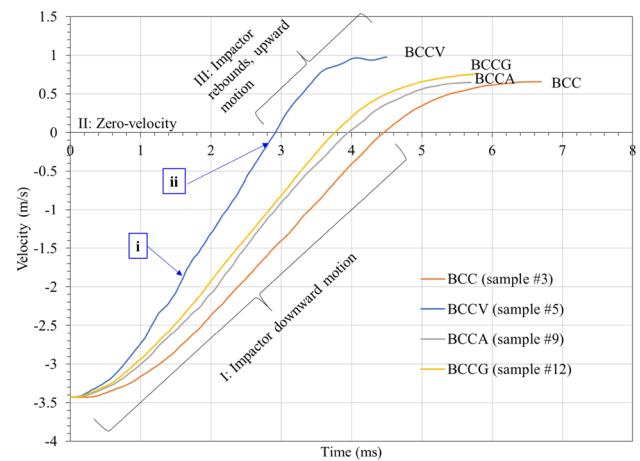


**Fig. 7** Comparison of typical velocity histories among all four configurations (samples 3, 5, 9, 12) impacted at 14.85 Joule

2.8 mm/s and 4.4 mm/s, respectively, and that for BCCA and BCCG samples are about 3.8–4.0 mm/s. The *Stage I* duration depends on the stiffness of the structure. Higher the stiffness lower is the time needed for the impactor to reach the maximum indentation depth. The compression behavior of the BCC, BCCV, BCCA, and BCCG samples presented in Ref. [24] shows that the BCCV and BCC have the highest and the lowest stiffnesses, respectively, while the BCCG and BCCA have similar stiffnesses. The most number of vertical struts in the BCCV structure offers the highest stiffness. The BCCA and BCCG samples have less number of vertical struts than BCCV (causing less stiffness than BCCV) while the BCC have the lowest stiffness. While the length of the response is different for the different configurations, the BCCV offers the higher velocity on the bounce in *Stage III* as compared to the other three configurations.

A second integration of the acceleration history in MATLAB provides a displacement history. The calculated displacement is for the impactor and it should be same as the deformation of the Kevlar and the ABS lattice core structure. Representative displacement curves for all four configurations are shown in Fig. 8. It is very clear from the figure that the BCCV has the least deformation while the BCC samples have the most. The BCCA and BCCG samples have the similar displacement history and lie between BCC and BCCV. Maximum deformations for all configurations and corresponding percentile coefficients of variance are summarized in Table 3. The BCC, BCCV, BCCA, and BCCG sandwich panel structure has average maximum deformations of 8.91, 5.99, 7.65, and 7.56 mm, respectively. Again Fig. 8 also shows three distinct stages I, II, and III that were discussed earlier. It is clear from Stage III in Fig. 8 that the BCC has the least elastic recovery and the BCCV has the most. The amount of elastic recovery for the BCCA and BCCG samples are similar and lies between

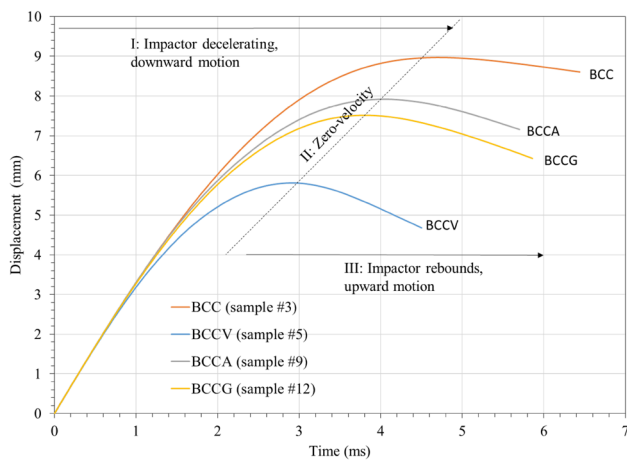


**Fig. 8** Comparison of typical displacement histories among all four configurations (samples 3, 5, 9, 12) impacted at 14.85 Joule

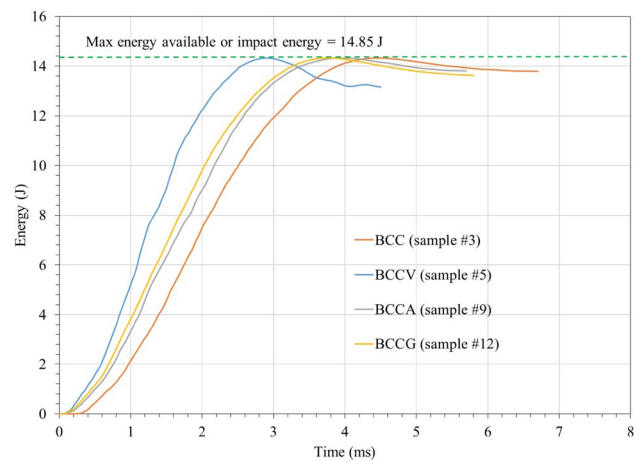


**Fig. 9** Comparison of typical energy histories among all four configurations (samples 3, 5, 9, 12) impacted at 14.85 Joule

BCC and BCCV. This trend in elastic recovery follows the trend of the stiffness [24] due to obvious reason.

The change in kinetic energy or energy transferred to the samples was calculated in Excel by using Eq. (3) and plotted against time during the impact period. The representative energy history is shown in Fig. 9. It is clear that the total transferred energy reaches the maximum available or impact energy at *Stage II* when the impactor is at its maximum displacement. However, some energy is recovered by the impactor during *Stage III* due to the elastic recovery of Kevlar face sheet and undamaged, elastically deformed lattice. After elastic recovery, the final transferred energy is the absorbed energy. Table 3 summarizes the average absorbed energy along with corresponding coefficient of variance in percentage. Although the four configurations have different total impact period, the BCC, BCCA, and BCCG samples have similar absorption energy of 13.83, 13.73, and 13.73 J, respectively. The BCCV samples have the lowest energy absorption of 13.05 J due to the largest elastic recovery. It may be mentioned here that a small portion of these absorbed energies are used to deform the Kevlar face sheets. Since the face sheets are thin, the energy needed to cause it to deform may well be

small. As such, the energy absorption behavior of LSs will still follow the same pattern.

Force history was obtained by multiplying the impactor mass with acceleration. Figure 10 shows the typical force history for all the four configurations. The plots have been smoothed for clarity. All the configurations show two peaks. The BCCV has the highest peak load followed by BCCG and BCCA, and BCC. The average peak loads for all configurations are summarized in Table 3 as well. The maximum load for the BCC, BCCV, BCCA, and BCCG specimens are 2447, 3669, 2838, and 2841 N, respectively. The peak loads appear to follow the peak load behaviors of the structures tested under compression load [24]. The first peak as indicated by [i] on the load–displacement curve correspond to the first stage of failure up to which the material deforms elastically deforms. This location is also shown in velocity history in Fig. 7 which indicates that the impactor is still moving in the downward direction within the LS. The second peak indicated by [ii] in Fig. 10 corresponds to the second stage of failure. This point is little before zero velocity as shown in Fig. 7. In other words, the impactor motion is still in the downward direction. The kinetic energy of the impactor decreases until the impactor velocity decreases to

**Table 3** Maximum displacement, peak load, and absorbed energy

Config.	Max displacement		Absorbed energy (impact energy = 14.85 J)		Peak Load from $F = ma$	
	Average (mm)	Coefficient of variance (%)	Average (J)	Coefficient of variance (%)	Average (N)	Coefficient of variance (%)
BCC	8.91	1.64	13.83	2.07	2447	0.79
BCCV	5.99	3.24	13.05	1.15	3669	2.92
BCCA	7.65	3.55	13.73	0.34	2835	5.49
BCCG	7.56	1.73	13.73	1.91	2841	2.35

Peak load was calculated from  $F = ma$

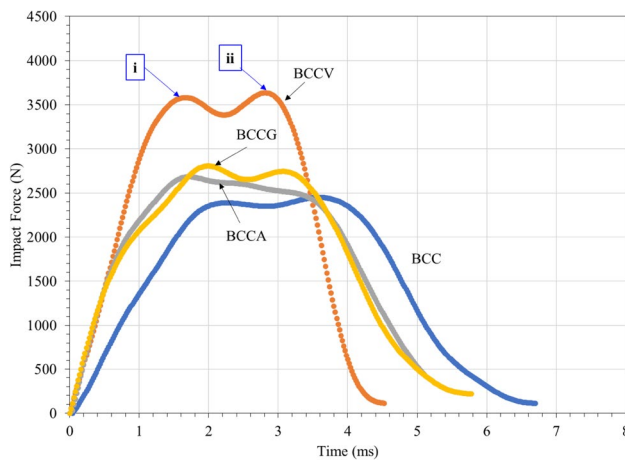


**Fig. 10** Comparison of typical force histories among for all four configurations calculated from  $F = ma$

zero. Subsequently, the elastic energy stored in the deformed LS and Kevlar face sheet causes the impactor to bounce back and the load approaches to zero where the impactor separates from the face sheet.

Figure 11 shows X-ray images of all four configurations after impact. The damage of internal lattice structures, and delamination at the face sheet/core interface are clearly visible. The depth and in-plane spread of impact damage has been quantified in the images as well. It is observed that the damage depths of BCC (Fig. 11a), BCCV (Fig. 11b), and BCCA (Fig. 11c) samples are 10.9 mm, 10.1 mm, and 10.6 mm, respectively. In other words, the top two layers of BCC, BCCV, and BCCA configurations failed while remaining two layers remained undamaged. On the other hand, the damage depth for BCCG samples is 8.5 mm, that means, top one and half layers failed keeping the remaining two and half layers undamaged. Damage sizes close to Kevlar for BCC,

BCCV, BCCA, and BCCG are 19.8 mm, 20.5 mm, 17.9 mm, and 16.0 mm, respectively.

Table 3 and Figs. 7, 8, 9 and 10 show that the BCCV configuration is the stiffest and strongest, while the BCC configuration is the most compliant and the weakest. The behavior of the BCCG and BCCA configurations is similar and fall between BCC and BCCV. The BCCA and BCCG have the same arrangement of vertical struts in the first two layers closest to the point of impact, namely no struts in the upper most layer and vertical struts at every node of the second layer (BCCA) and vertical struts at half the nodes in the second layer (BCCG). The struts in the second layer seem to provide constraints to the deformation for both structures, and therefore similar behavior. This observation is confirmed by the X-ray images discussed in Fig. 11.

## Summary

In this study, the low-velocity impact behavior of 3D-printed polymer lattice structures has been investigated. The differences in the absorption energy has been discussed for comparison of the four configurations which are the BCC, BCCV, BCCA and BCCG. To consider uncertainty of the results, three specimens were used for each configuration. The differences in design between the four configurations were based on the strut distribution inside the unit cells. In contrast, there are no vertical struts in the BCC configuration. A CAD software has been used to design the specimens. A 3D printer which is Stratasys uPrint 3D has been used to fabricate the specimen. The specimens were investigated under a low-velocity impact test using an ASTM Standard D7136. Furthermore, the sandwich panel was designed and fabricated for impact tests. Four ply Kevlar

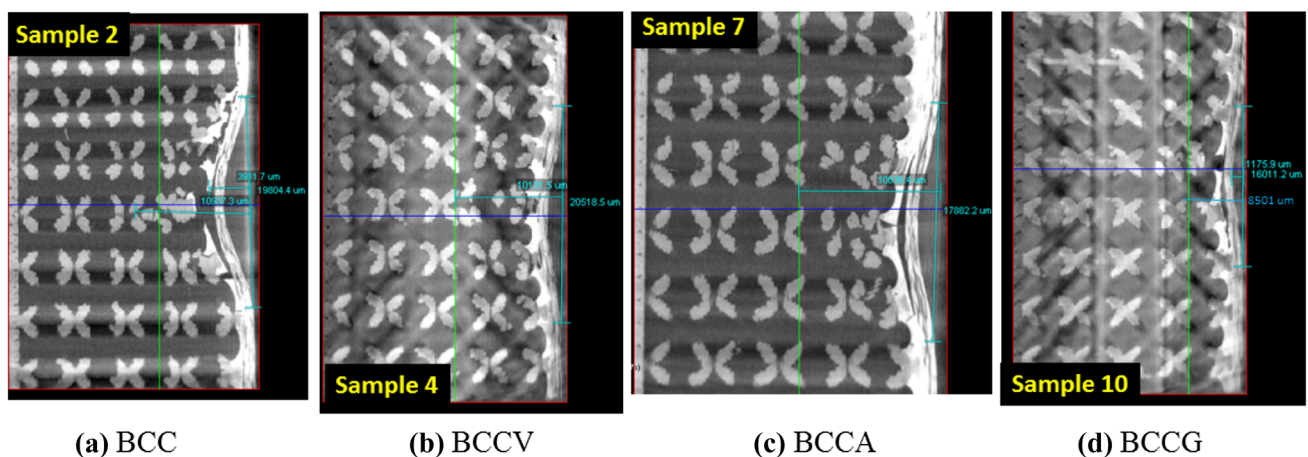


**Fig. 11** X-ray images of four different impacted samples



face sheets were fabricated and cured using hot press and then glued to the lattice core structures.

The data obtained from the accelerometer attached with the impactor were integrated to find impactor velocity and displacement. The absorption energy was calculated from the change in impactor kinetic energy. BCCV had the lowest penetration compared with others. The BCCV have the lowest energy absorption capability while the other three configurations have similar energy absorption capability when the impact energy is 14.85 J.

## References

1. Nguyen DS (2016) A method to generate lattice structure for additive manufacturing. pp 966–970
2. Dhaliwal GS, Newaz GM (2016) Modeling low velocity impact response of carbon fiber reinforced aluminum laminates (CAR-ALL). *J Dyn Behav Mater* 2:181–193
3. Ju J, Summers JD, Ziegert J, Fadel G (2012) Design of honeycombs for modulus and yield strain in shear. *J Eng Mater Technol* 134(1):011002
4. Hundley JM, Clough EC, Jacobsen AJ (2015) The low velocity impact response of sandwich panels with lattice core reinforcements. *Int J Impact Eng* 84:64–77
5. Mines RAW, Tsopanos S, Shen Y, Hasan R, McKown ST (2013) Drop weight impact behaviour of sandwich panels with metallic micro lattice cores. *Int J Impact Eng* 60:120–132
6. Shen Y, Cantwell W, Mines R, Li Y (2014) Low-velocity impact performance of lattice structure core based sandwich panels. *J Compos Mater* 48(25):3153–3167
7. Zhao W, Xie Z, Li X, Yue X, Sun J (2018) Compression after impact behavior of titanium honeycomb sandwich structures. *J Sandwich Struc Mater* 20(5):639–657
8. Williams CB. Design and development of layer-based additive manufacturing process for realization of metal parts of designed mesostructure. Ph.D. Dissertation, Georgia Institute of Technology 2008. <https://smartech.gatech.edu/handle/1853/22687?show=full>. Accessed 10 July 2018
9. Turner AJ, Al Rifaie M, Mian A, Srinivasan R (2018) Low-velocity impact behavior of sandwich structures with additively manufactured polymer lattice cores. *J Mater Eng Perform* 27(5):2505–2512
10. Vitale M, Cotteleer M, Holdowsky J (2016) An overview of additive manufacturing (cover story). *Def AT&L* 45(6):6–13
11. Neitzert TR (2015) Accuracy of additive manufactured parts. *Key Eng Mater* 661:113–118
12. June FA (2017) Acta technica corviniensis–bulletin of engineering compressive properties of commonly used
13. Saadlaoui Y, Milan JL, Rossi JM, Chabrand P (2017) Topology optimization and additive manufacturing: comparison of conception methods using industrial codes. *J Manuf Syst* 43:178–186
14. Ben-Ner A, Siemsen E (2017) Decentralization and localization of production. *Calif Manage Rev* 59(2):5–23
15. Bagsik A, Schöppner V (2011) Mechanical properties of fused deposition modeling parts manufactured with ULTEM 9085. *Proc ANTEC* 2011:1294–1298
16. Su H, McConnell J (2011) Influences of material properties on energy absorption of composite sandwich panels under blast loads. *J Compos Constr* 16(4):464–476
17. St-Pierre L, Deshpande VS, Fleck NA (2015) The low velocity impact response of sandwich beams with a corrugated core or a Y-frame core. *Int J Mech Sci* 91:71–80
18. Vesenjok M, Ren Z, Öchsner A (2008) Behaviour of cellular materials under impact loading. *Mater Sci Eng Technol* 39(2):125–132
19. Bao Jin-Biao, Weng Geng-Sheng, Zhao Ling, Liu Zhi-Feng, Chen Zhong-Ren (2014) Tensile and impact behavior of polystyrene microcellular foams with bi-modal cell morphology. *J Cell Plast* 50(4):381–393
20. Stratasys. uPrint SE Plus (2018) <http://www.stratasys.com/3d-printers/uprint-se-plus>. Accessed 21 Feb 2018
21. Stratasys. ABSplus (2018) <http://www.stratasys.com/materials/search/absplus>. Accessed 21 Feb 2018
22. Vidakis N, Petousis M, Vairis A, Savvakis K, Maniadi A (2017) On the compressive behavior of an FDM Steward Platform part. *J Comput Des Eng* 1:339–346
23. Turner AJ (2018) Low-Velocity Impact Behavior of Sandwich Panels with 3D Printed Polymer Lattice Core Structures.” MS Thesis, Wright State University, 2017. [https://etd.ohiolink.edu/etd.send\\_file?accession=wright1496345616948541&disposition=inline](https://etd.ohiolink.edu/etd.send_file?accession=wright1496345616948541&disposition=inline). Accessed 10 July 2018
24. Al Rifaie M, Mian A, Srinivasan R (2018) Compression behavior of three-dimensional printed polymer lattice structures. *J Mater*. <https://doi.org/10.1177/1464420718770475>

**Publisher's Note** Springer Nature remains neutral with regard to jurisdictional claims in published maps and institutional affiliations.